HHS Public Access

Author manuscript

Nat Cell Biol. Author manuscript; available in PMC 2015 September 01.

Published in final edited form as:

Nat Cell Biol. 2015 March ; 17(3): 322–332. doi:10.1038/ncb3121.

FBXW7 modulates cellular stress response and metastatic potential via HSF1 post-translational modification

Nikos Kourtis[#1,2], **Rana S. Moubarak**[#3,4], **Beatriz Aranda-Orgilles**[1,2], **Kevin Lui**[4,6], **Iraz T. Aydin**[5], **Thomas Trimarchi**[1,2], **Farbod Darvishian**[3,4], **Christine Salvaggio**[4,6], **Judy Zhong**[4,9,10], **Kamala Bhatt**[1,2], **Emily I. Chen**[7], **Julide T. Celebi**[5], **Charalampos Lazaris**[1,2,8], **Aristotelis Tsirigos**[1,8], **Iman Osman**[4,6,11], **Eva Hernando**[3,4,11], and **Iannis Aifantis**[1,2,11]

[1]Howard Hughes Medical Institute and Department of Pathology, NYU School of Medicine, New York, NY 10016, USA.

[2]NYU Cancer Institute and Helen L. and Martin S. Kimmel Center for Stem Cell Biology, NYU School of Medicine, New York, NY 10016, USA.

[3]Department of Pathology, NYU School of Medicine, New York, NY 10016, USA.

[4]Interdisciplinary Melanoma Cooperative Group, NYU Cancer Institute, New York, NY 10016, USA.

[5]Departments of Pathology and Dermatology, Icahn School of Medicine at Mount Sinai, New York, NY 10029, USA.

[6]Ronald O. Perelman Department of Dermatology, NYU School of Medicine, New York, New York, NY 10016, USA.

[7]The Herbert Irving Comprehensive Cancer Center, Department of Pharmacology, Columbia University Medical Center, New York, NY 10032, USA.

[8]Center for Health Informatics and Bioinformatics, NYU School of Medicine, NY 10016, USA.

[9]Department of Population Health, New York University School of Medicine, New York, New York

[10]Department of Environmental Medicine, New York University School of Medicine, New York, New York

[#] These authors contributed equally to this work.

[11]Correspondence to: Iannis.aifantis@nyumc.org (I.A), Eva.Hernando-Monge@nyumc.org (E.H) or Iman.Osman@nyumc.org (I.O).

Author Contributions I.A. and N.K. designed the experiments, analyzed the data and wrote the manuscript. N.K. performed the bulk of the experiments. R.S.M. performed the melanoma invasion and metastasis experiments. B.A.O. performed the FBXW7 mass-spectrometry experiment and analyzed the mass-spectrometry data. I.T.A., T.T., K.L. and K.B. performed experiments. F.D. scored the primary melanoma samples. C.S and J. Z analyzed patient data. E.I.C. analyzed the mass-spectrometry data. I.O., E.H. and J.T.C. provided melanoma-related materials and contributed with ideas. A.T. and C.L. performed the analysis of genome-wide data.

The authors declare that they have no competing financial interests.

Supplementary Information accompanies this manuscript

Deposited data accession numbers

The datasets generated for this study can be accessed at GEO (GSE57399). Previously published data sets re-analyzed for this study include microarray data from normal skin, primary and metastatic melanoma[58] which can be accessed at GEO (GSE7553); and array-CGH profiles from primary and metastatic melanoma[44] which can be accessed at GEO (GSE7606).

Abstract

Heat-shock factor 1 (HSF1) orchestrates the heat-shock response in eukaryotes. Although this pathway has been evolved to help cells adapt in the presence of challenging conditions, it is co-opted in cancer to support malignancy. However, the mechanisms that regulate HSF1 and thus cellular stress response are poorly understood. Here we show that the ubiquitin ligase FBXW7 α interacts with HSF1 through a conserved motif phosphorylated by GSK3β and ERK1. FBXW7α ubiquitylates HSF1 and loss of FBXW7α results in impaired degradation of nuclear HSF1 and defective heat-shock response attenuation. FBXW7α is either mutated or transcriptionally downregulated in melanoma and HSF1 nuclear stabilization correlates with increased metastatic potential and disease progression. FBXW7α deficiency and subsequent HSF1 accumulation activates an invasion-supportive transcriptional program and enhances the metastatic potential of human melanoma cells. These findings identify a post-translational mechanism of regulation of the HSF1 transcriptional program both in the presence of exogenous stress and in cancer.

Organisms respond to stressors by activating adaptive mechanisms to restore homeostasis. Environmental and intrinsic factors elicit the highly conserved heat-shock response, orchestrated by the transcription factor HSF1. Upon stress, HSF1 induces gene expression of heat-shock proteins (HSPs), which act as molecular chaperones and restore protein homeostasis[1-3]. It has long been noted that cancer cells bolster their chaperone system to cope with stress caused by increased protein production due to aneuploidy, increased protein folding requirements and proteasome overwhelming[4]. HSF1 deficiency protects against tumorigenesis driven by different oncogenic stimuli[5-7]. In addition, depletion of HSF1, which itself is not a *bona fide* oncogene, decreases the viability of multiple cancer cell lines, a phenomenon coined as “non-oncogene addiction”[6-13]. Apart from its classic role as a major activator of chaperone-encoding genes, HSF1 also regulates a malignant-specific transcriptional program, critical for cancer cells and tumor microenvironment[14-16]. However, the signaling pathways modulating the HSF1 cancer-specific activity remain unknown.

Heat-shock response activation-attenuation is an intricate process as the HSF1 protein undergoes extensive post-translational modifications[17-19]. Protein stability controlled by the ubiquitinproteasome pathway is an emerging theme in human cancer. FBXW7, a substrate-targeting subunit of the SCF (Skp1-Cul1-F box) ubiquitin ligase complex[20] targets several key regulators of proliferation, growth and apoptosis for proteasomal degradation[21-29]. *FBXW7* is mutated in a significant portion of diverse human cancers[30]. We investigate here the mode of post-translational regulation of HSF1 and demonstrate an interaction between FBXW7 and HSF1. We show that FBXW7α controls the stability of nuclear HSF1 and modulates the attenuation phase of the heat-shock response. Moreover, FBXW7 deficiency enhances the metastatic ability of melanoma via HSF1 stabilization and alteration of the HSF1 malignant transcriptional program. Altogether, our data suggest that a tumor suppressor, FBXW7, regulates heat-shock response and cancer cell stress response and metastatic potential via modification of HSF1.

HSF1 is a substrate of the FBXW7α ligase

To identify substrates of the ubiquitin ligase FBXW7α, we performed tandem affinity purification of FBXW7α and identified its interacting proteins by 2D LC-MS/MS (Fig. 1a; Supplementary Table 1). Interestingly, HSF1, similar to MYC, was detected in FBXW7α immunoprecipitates (Fig. 1b). However, the HSF1 interaction with a WD40 domain mutant FBXW7α, that lacks the ability to bind protein substrates but binds the Cullin 1 complex, was significantly reduced (Fig. 1b). In addition, endogenous FBXW7 and HSF1 were found to interact (Supplementary Fig. 1a). Analysis of HSF1 protein sequence revealed the presence of two conserved amino-acid sequences resembling the canonical FBXW7 degradation motif (degron) S/TPPXS/T[20], one of which (SPPQS), contains evolutionary conserved phosphoamino acids (Fig. 1c).

We next mapped the FBXW7α -binding motif of human HSF1. To investigate which amino acids participate in the interaction of HSF1 with FBXW7α, we mutated the two putative FBXW7α degrons (amino acid positions 303-307 and 363-367). We found that an HSF1 mutant containing alanine substitutions at both Ser303 and Ser307 [HSF1(Ser303/307Ala)] failed to bind FBXW7α (Fig. 2a). Further mutational analysis revealed both Ser303 and Ser307 as necessary residues contributing to its interaction with FBXW7α (Fig. 2b). Notably, phosphorylation of HSF1 on Ser303/307 by GSK3β and ERK1 respectively, has been suggested to play a role in down-modulating HSF1's activity during recovery from stress[31-36]. Treatment of cells with a GSK3 inhibitor (GSK3i IX and XVI) or a MEK inhibitor (U0126) markedly decreased the affinity of FBXW7α for HSF1 (Fig. 2c, d; Supplementary Fig. 1b). This is consistent with the notion of a priming role for the Ser307 phosphorylation for subsequent phosphorylation on Ser303[37]. Moreover, depletion of *FBXW7* increased the half-life of nuclear HSF1 (Fig. 2e).

Finally, we tested the ubiquitylation status of HSF1. Upon heat stress, HSF1 poly-ubiquitylation was markedly increased, suggesting a tagging mechanism for rapid proteasomal degradation upon stress removal (Fig. 2f; Supplementary Fig. 1c). In sharp contrast, induced HSF1 polyubiquitylation was significantly reduced upon *FBXW7* silencing (Fig. 2f; Supplementary Fig. 1c), suggesting that FBXW7 binds and directly controls HSF1 ubiquitylation.

Loss of *FBXW7* leads to defective nuclear HSF1 clearance and prolonged heat-shock response

To determine whether FBXW7 affects HSF1 protein turnover, we utilized the human colorectal cancer cell line HCT116, an isogenic cell line containing a homozygous deletion (KO) of the *FBXW7* gene and its wild type (WT), *FBXW7*-expressing counterpart[38]. HSF1 shuttles between the cytoplasm and the nucleus, but upon stress it accumulates in the nucleus[19, 39]. Subcellular fractionation analysis of HSF1 revealed identical cytoplasmic HSF1 protein levels in WT and *FBXW7* KO cells under basal conditions (37°C; Supplementary Fig. 2a). Strikingly, increased baseline HSF1 nuclear levels were observed in *FBXW7* KO cells, compared to WT cells (Fig. 3a), in agreement with the nuclear localization of FBXW7α protein. Next, we exposed both cell lines to heat shock and noticed

a marked increase of nuclear HSF1 levels. We also observed a rapid reduction of nuclear HSF1 during the recovery period, in WT cells (Fig. 3a). In contrast, we noted a prolonged stabilization of nuclear HSF1 in *FBXW7* KO cells (Fig. 3a). HSF1 mRNA levels did not change during heat shock or recovery (Supplementary Fig. 2b). Subsequently, we asked whether loss of *FBXW7* affects the clearance of nuclear HSF1, accumulated upon exposure to MG132, a known proteotoxic stressor. We observed reduced degradation of HSF1 in *FBXW7* KO cells, compared to WT cells, upon MG132 removal (Fig. 3b). However, we could not detect any significant difference in the cytoplasmic fraction (Supplementary Fig. 2c). Thus, FBXW7 deficiency results in defective clearance of nuclear HSF1 upon exogenous stress removal.

We then hypothesized that stabilization of nuclear HSF1 in *FBXW7* deficient cells might affect HSF1 target gene expression upon stress removal. We heat shocked the HCT116 WT and *FBXW7* KO cells (42°C for 1 hour) and monitored the expression of the heat-shock-inducible *HSPA6* gene after 2 hours of recovery at 37°C. In WT cells, *HSPA6* expression was diminished during the recovery period. Strikingly, in the *FBXW7* KO cells, *HSPA6* expression was higher after recovery, compared to heat shock (Supplementary Fig. 3a). Identical results were obtained in HEK293T cells upon *FBXW7* silencing (Supplementary Fig. 3b). To assess the change of HSF1 targets expression after heat shock and recovery, in a high throughput approach, RNA sequencing (RNA-Seq) was performed in HCT116 WT and *FBXW7* KO cells. To identify direct HSF1 targets, we first performed chromatin immunoprecipitation coupled to high-throughput sequencing (ChIP-Seq) for HSF1 after heat-shock treatment of HCT116 (WT and KO) cells. We focused on high-confidence HSF1 targets and monitored their expression during heat shock and recovery in the two cell lines. In contrast to WT cells, the expression of positively regulated HSF1 targets, such as *HSPH1*, *HSPB1* and *HSPE1*, continued to increase in *FBXW7* KO cells during recovery from heat shock (Fig. 3c). Notably, the majority of common HSF1 heat-shock response targets (both positively and negatively regulated) in HCT116 WT and *FBXW7* KO cells displayed opposite expression pattern during recovery from heat-shock treatment (Fig. 3c). However, *HSF1* was expressed at similar basal levels in the two cell lines (Supplementary Fig. 3c). Thus, *FBXW7* loss results in defective attenuation of the heat-shock response.

Loss of *FBXW7* leads to aberrant HSF1 genome occupancy and protects cells from proteotoxic stress

To determine whether altered HSF1 stability can control genome occupancy by this transcription factor and subsequently alter HSF1 regulated transcriptional profiles, we performed ChIP-Seq analysis in WT and *FBXW7* KO HCT116 cells under basal conditions. A small (52) number of gene loci were bound by HSF1 in HCT116 WT cells. In contrast, in the *FBXW7* KO cells we identified a much larger number (485) of genes bound by HSF1 (Fig. 3d), suggesting that HSF1 protein increased stability leads to new binding sites on the genome (Fig. 3e, *EIF4A2*, *CCT6A*). The vast majority of genes bound by HSF1 in WT cells were also bound in *FBXW7* KO cells. Notably, however, for many of the genes bound in both cell lines, promoter HSF1 binding (as defined by the peak density) was significantly stronger in the *FBXW7* KO cells compared to WT cells (Fig. 3e, *HSPD1/E1*, *HSP90AB1*;

3f). Stronger binding of HSF1 in *FBXW7* KO cells translated to higher expression of common with WT target genes (Fig. 3g).

To assess the functional significance of the altered HSF1 transcriptional program in the *FBXW7* KO cells, we asked whether these cells have a survival advantage in the presence of proteotoxic stress. We monitored cell survival over 3 days in the presence of sublethal concentrations of the proteasome inhibitor MG132 and the HSP90 inhibitor Radicicol. *FBXW7* KO cells were significantly more resistant to both proteotoxic stressors, compared to WT cells (Supplementary Fig. 4a). To test the FBXW7-HSF1 interplay in a non-cancer context, we examined mouse embryonic fibroblasts (MEFs) isolated from *Fbxw7* conditional knockout mice[40]. We observed nuclear accumulation in $Fbxw7^{-/-}$ MEFs compared to $Fbxw7^{flox/flox}$ and WT counterparts (Supplementary Fig. 4b). We then assessed MEF survival upon exposure to proteotoxic drugs. We found that $Fbxw7^{-/-}$ MEFs displayed increased survival compared to $Fbxw7^{flox/flox}$ and WT MEFs (Supplementary Fig. 4c). Notably, the survival advantage was abolished upon downregulation of HSF1, indicating a stringent HSF1 requirement for protection against proteotoxicity (Supplementary Fig. 4c).

HSF1 protein levels and gene target expression are associated with metastasis in melanoma

To further investigate the role of FBXW7-HSF1 interplay in human cancer progression and metastasis, we focused on melanoma, a solid tumor in which *FBXW7* is frequently mutated and inactivated[23, 30, 41]. We tested HSF1 protein expression using immunohistochemistry in human specimens. We found that HSF1 protein levels were significantly increased as melanoma progressed to metastatic disease ($P<0.001$ for metastatic versus primary or nevi) (Fig. 4a). To assess the functional significance of HSF1 accumulation in melanoma, we asked whether HSF1 gene targets were upregulated during disease progression. Previously characterized HSF1 targets, including *HSPD1*, *HSPE1*, *HSPH1* and *CKS2* were expressed in significantly higher levels in metastatic melanoma compared to primary melanoma and normal skin (Fig. 4b). In contrast, *FBXW7* expression was significantly reduced in metastatic melanoma, while *HSF1* mRNA expression did not change significantly (Fig. 4b), suggesting post-translational regulation. In agreement with this model, we found that FBXW7 protein expression shows opposite pattern to HSF1 expression during disease progression (Figure 4c). To further investigate the hypothesis that HSF1 activation is associated with poor disease outcome, we expanded the primary human melanoma specimens cohort. These tumors were scored for levels of HSF1 and survival outcomes were investigated. Melanoma patients whose primary tumor expressed high levels of nuclear HSF1 had significantly decreased recurrence-free survival relative to the patients with low HSF1 levels ($P=0.01$, median follow up 5 years; Fig. 4d). These studies connect the FBXW7:HSF1 interaction to melanoma metastasis and disease progression.

Finally, to investigate the direct link between HSF1-regulated gene signature and *FBXW7*α expression, we analyzed human melanoma cases from the Cancer Genome Atlas (TCGA) and generated an HSF1 “gene signature” comprised of mRNAs positively or negatively correlated with HSF1 levels. HSF1 transcription factor exerts both positive and negative role

on the regulation of its targets and mRNAs positively correlated with HSF1 expression comprised the “positive signature” while mRNAs negatively correlated with HSF1 expression comprised the “negative signature”. In complete agreement with our proposed model, the HSF1 “positive signature” is negatively correlated with *FBXW7*α expression ($P<0.001$), while the “negative signature” is positively associated with *FBXW7*α expression ($P<0.001$; Fig. 4e).

FBXW7 controls HSF1 protein stability in human melanoma

We next monitored a panel of melanoma cell lines for nuclear HSF1 levels. Notably, melanoma cells deficient for *FBXW7* (WM39, WM3862, WC00125) had significantly higher levels of nuclear HSF1, compared to WT cell lines (SKMEL24, SKMEL5, SKMEL28, COLO829; Fig. 5a). Furthermore, *FBXW7* siRNA-mediated knockdown resulted in nuclear HSF1 accumulation in 501mel melanoma cell line (Fig. 5b). Interestingly, *FBXW7* knockdown did not have any effect on cytoplasmic HSF1 levels (Supplementary Fig. 5a). We reasoned that the increased HSF1 nuclear accumulation upon *FBXW7* knockdown might translate to elevated expression of HSF1 gene targets. Indeed, we were able to show increased expression of classical-HSF1 targets upon *FBXW7* knockdown (Fig. 5c; Supplementary Fig. 5b).

As we demonstrated earlier, the FBXW7:HSF1 interaction and substrate degradation requires phosphorylation of HSF1 by GSK3β and ERK1 (Fig. 2c, d). The RAS/RAF/MEK/ERK signaling pathway is hyperactivated in a large fraction of human melanoma[42]. To test whether the BRAF/MEK inhibition results in alteration of HSF1 protein levels, we treated the BRAF mutant cell line 451Lu with the BRAF inhibitor Vemurafenib and the MEK inhibitor Trametinib. We observed stabilization of nuclear HSF1 upon treatment with either inhibitor (Fig. 5d). In contrast, cytoplasmic HSF1 levels remained unaffected upon treatment (Supplementary Fig. 5c).

To investigate whether *FBXW7* deficient melanoma cells show aberrant nuclear HSF1 clearance upon exogenous stress removal, we heat shocked WT (SKMEL28) and *FBXW7* deficient (WM39) cells and monitored nuclear HSF1 levels. Both cell lines mounted an efficient heat-shock response as indicated by the accumulation of nuclear HSF1 (Supplementary Fig. 5d). During recovery, in SKMEL28 cells, nuclear HSF1 levels returned to untreated levels. In sharp contrast, in *FBXW7*-deficient WM39 cells, nuclear HSF1 levels remained stable during the recovery period (Supplementary Fig. 5d). Overexpression of *FBXW7*α partially restored HSF1 degradation during recovery (Supplementary Fig. 5d).

Accumulation of nuclear HSF1 upon *FBXW7* loss enhances the metastatic potential in human melanoma

In a recent comparative genomic screen for the identification of oncogenic metastasis drivers[43] HSF1 was suggested to be pro-invasive. We hypothesized that downregulation of *FBXW7*, and consequently stabilization of HSF1, may impact metastasis in human melanoma. To test this hypothesis, we assessed *in vitro* the invasive capacity of melanoma cells upon *FBXW7* knockdown. Notably, downregulation of *FBXW7* resulted in significantly

increased invasion in the melanoma cell line 451Lu, compared to control cells (Fig. 5e). In agreement with this finding, *FBXW7* downregulation transformed the non-invasive melanoma cell line SKMEL239 into highly invasive (Fig. 5e). As a control, *FBXW7* downregulation had no effect on the invasive capacity of A375 cells that express negligible levels of nuclear HSF1 (Fig. 5e). Cytoplasmic HSF1 levels were comparable in all cell lines (Supplementary Fig. 5e). Finally, to test whether HSF1 function is critical for the survival of melanoma, we modulated *HSF1* expression using a previously validated shRNA[7]. The viability of nuclear *HSF1*-expressing 451Lu melanoma cells was strongly affected by the *HSF1* silencing (Fig. 5f; Supplementary Fig. 5f, g). In sharp contrast, A375 cells were largely unaffected by *HSF1* depletion (Fig. 5f; Supplementary Fig. 5f, g). Collectively, our data suggest that HSF1 is a critical substrate of FBXW7 and its accumulation upon *FBXW7* downregulation modulates the invasive capacity of melanoma cells that are “addicted” to HSF1 for survival.

To investigate the effect of *FBXW7* downregulation and subsequent nuclear HSF1 accumulation on metastatic capacity of melanoma *in vivo*, 451Lu cells transduced with *shFBXW7* or sh*LUC* were injected into immune-compromised recipient mice. Although *FBXW7* knockdown did not affect primary tumor growth (Fig. 6a, b; Supplementary Fig. 6a), it led to dramatic increase in the formation of metastatic foci in the lungs (Fig. 6c, d). Primary tumors consisting of melanoma cells carrying *shFBXW7* exhibited prominent nuclear HSF1 staining compared to their control counterparts. Ki-67 staining did not reveal any difference in proliferation rates between the two treatments (Fig. 6e). Also, *FBXW7* downregulation did not affect differentiation of melanoma cells (Supplementary Fig. 6b).

To verify that accumulation of other reported FBXW7 substrates does not impact the increased metastatic potential of melanoma cells upon *FBXW7* depletion, we examined a panel of known substrates. Of the substrates tested, downregulation of *FBXW7* resulted in significant stabilization of only HSF1 and Cyclin E in 451Lu cells (Supplementary Fig. 7a). Similar stabilization of Cyclin E upon *FBXW7* downregulation was observed in the “non-HSF1 addicted” cell line A375, suggesting that nuclear accumulation of Cyclin E is not sufficient to alter the metastatic potential of melanoma cells (Supplementary Fig. 7b; Fig. 5e). In addition, overexpression of Cyclin E did not increase the invasive capacity of melanoma cells (Supplementary Fig. 7c), suggesting that HSF1 is the key FBXW7 substrate controlling melanoma metastasis.

We hypothesized that depletion of *HSF1* may abolish the increased metastatic potential of melanoma cells with reduced *FBXW7* expression. To test this hypothesis, we utilized the *in vitro* invasion system and used hairpins that only partially silence HSF1 to avoid the acute effects on cell survival. We were able to show that HSF1 deficiency completely suppressed the increased invasive potential of melanoma cells with reduced *FBXW7* expression (Fig. 6f; Supplementary Fig. 7d, e). In contrast, *Cyclin E* (*CCNE1*) downregulation had no significant effect on invasion (Fig. 6f; Supplementary Fig. 7d, e). These studies connect the FBXW7:HSF1 module to human cancer metastasis and invasion.

HSF1 orchestrates a metastasis-promoting transcriptional program in melanoma

To gain insights into the molecular basis of HSF1 metastasis-supportive transcriptional program, we performed HSF1 ChIP-Seq analysis using the 451Lu melanoma cells. Initial analysis suggested a preference for promoter binding (Fig. 7a). Gene enrichment analysis (GSEA) of HSF1 targets using publicly available data[44] revealed significant enrichment for gene sets containing genes significantly altered in metastatic relative to primary melanomas (Fig. 7a, b). To better focus on *bona fide* melanoma metastasis regulators, we exploited recent studies that described a number of pro-invasive and oncogenic genes in melanoma[43]. Strikingly, our analysis revealed that several of these invasion/metastasis drivers are directly bound by HSF1 (Fig. 7b; MTHFD2, HMGB1 and ITGB3BP). We hypothesized that nuclear HSF1 accumulation upon *FBXW7* knockdown may result in upregulation of the melanoma transcriptional program. To test this hypothesis, we monitored the expression of selected metastasis-related HSF1 targets, upon *FBXW7* knockdown. *FBXW7* silencing resulted in significant upregulation of such HSF1 targets (Fig. 7c). Based on these findings, we suggest that HSF1 orchestrates a metastasis-supportive transcriptional program that is bolstered upon nuclear accumulation due to *FBXW7* deficiency/mutation.

DISCUSSION

The present study sheds light on the regulation of the heat-shock response pathway attenuation phase through modulation of HSF1 stability by the ligase FBXW7. Moreover, it illustrates that FBXW7 modulates the malignant transcriptome via stabilization of HSF1. Since HSF1 provides critical stress relief and metastatic advantage in cancer, it is tempting to speculate that HSF1 stabilization is an important arm of the FBXW7 tumor suppressor activity in all tumors where *FBXW7* mutations and genomic loses are reported. Also, given that *FBXW7* function is frequently impaired in cancer by mechanisms other than mutations and allelic loss[41, 45, 46], we propose that the impact of HSF1 stabilization on cancer progression is broad.

Despite decades of study, HSF1 regulation during classic heat-shock response is not fully understood. The extensive array of post-translational modifications of HSF1 during the activation/attenuation cycle adds complexity. In the light of current knowledge, attenuation of the heat-shock response pathway involves weak interactions of HSF1 with HSPs and SIRT1-dependent control of HSF1 DNA binding activity[47-50]. Recently, a genome-wide RNAi screen suggested that the nuclear proteasome has a pivotal role in the regulation of the heat-shock response[51]. However, no specific ubiquitin complex was previously connected to HSF1 ubiquitylation. We were able to show here that FBXW7 links the activated HSF1 to the degradation machinery and FBXW7 activity affects both the classical role of HSF1 in the heat-shock response and its role in the orchestration of the cancer-supportive transcriptome (Supplementary Fig. 7f). It has been previously shown that HSF1 amino acids at positions 303 and 307 are important for the down-modulation of the heat-shock response[31-36]. Our study shows that these amino acids mediate the interaction of HSF1 with the CUL1:FBXW7 ubiquitylation complex. Importantly, we show that this interaction is

controlled by molecular pathways frequently deregulated in cancer (GSK3β, ERK1). Since HSF1 is a powerful modifier of tumorigenesis[7, 52], it remains to be seen whether altered function of these kinases in different cancers converges on HSF1 stability.

Previous studies have suggested that HSF1 activation is associated with poor outcome in breast cancer[39]. Interestingly, reduced *FBXW7* expression or inactivating mutations is significantly correlated with poor patient prognosis in multiple cancers [41, 53-56]. Our data unify these observations and prove that HSF1 accumulation due to *FBXW7* altered expression provides an advantage in cancer cells during disease progression. Indeed, we show a direct correlation between FBXW7 and HSF1 protein expression to increased metastatic potential and decreased recurrence-free survival of melanoma patients. These data suggest that HSF1 could be a biomarker and a therapeutic target in this disease.

METHODS

Protein Immunoprecipitation

HEK293 were treated for 6 h with 10 μM MG132 to allow the accumulation of FBXW7 interacting proteins. Cells were then lysed in lysis buffer (50 mM Tris-HCl, ph 7.5, 150 mM NaCl and 2 mM EDTA) containing invitrosol (Invitrogen), PMSF, NaF, NaVO3 and proteinase inhibitors (Sigma). Tandem purification was performed. First immunoprecipitation was carried out overnight with anti-FLAG agarose beads. Next day, beads were washed and FLAG-HA-FBXW7 was eluted with 3xFLAG peptide. The eluate was used for a second immunoprecipitation with anti-HA agarose beads. Beads were thoroughly washed and subsequently digested for MS analysis.

Trypsin Digestion for MS Analysis

50 μl of 50 mM Ammonium Bicarbonate solution were added to the beads for trypsin digestion. 2 μg of trypsin was added to each sample along with 2 mM $CaCl_2$ and incubated at 37°C for 16 hours. Samples were centrifuged subsequently for 30 min at 14,000 rpm, and the supernatants were transferred to fresh tubes to be acidified with 90% formic acid (2% final) to stop proteolysis. The soluble peptide mixtures were collected for LC-MS/MS analysis.

Multidimensional Protein Identification Technology (MudPIT) and Tandem Mass Spectrometry

Peptide mixtures were pressure-loaded onto a 250 μm inner diameter (i.d.) fused-silica capillary packed first with 3 cm of 5 μm strong cation exchange material (Partisphere SCX, Whatman), followed by 3 cm of 10 μm C18 reverse phase (RP) particles (Magic C18 AQ 3 μm, Michrom. Bioresources, Auburn, CA). Loaded and washed microcapillaries were connected *via* a 2 μm filtered union (UpChurch Scientific) to a 100 μm i.d. column, which had been pulled to a 5 μm i.d. tip using a P-2000 CO_2 laser puller (Sutter Instruments), then packed with 13 cm of 3 μm C18 reverse phase (RP) particles (Magic C18 AQ 3 μm, Michrom. Bioresources, Auburn, CA) and equilibrated in 5% acetonitrile, 0.1 % formic acid (Buffer A). This split-column was then installed inline with a NanoLC Eskigent HPLC pump. The flow rate of channel 2 was set at 300 nl/min for the organic gradient. The flow

rate of channel 1 was set to 0.5 μl/min for the salt pulse. Fully automated 11-step chromatography runs were carried out. Three different elution buffers were used: 5% acetonitrile, 0.1% formic acid (Buffer A); 98% acetonitrile, 0.1% formic acid (Buffer B); and 0.5 M ammonium acetate, 5% acetonitrile, 0.1% formic acid (Buffer C). In such sequences of chromatographic events, peptides are sequentially eluted from the SCX resin to the RP resin by increasing salt steps (increase in Buffer C concentration), followed by organic gradients (increase in Buffer B concentration). The last chromatography step consists in a high salt wash with 100% Buffer C followed by acetonitrile gradient. The application of a 2.5 kV distal voltage electrosprayed the eluting peptides directly into a LTQ-Orbitrap XL mass spectrometer equipped with a nano-LC electrospray ionization source (ThermoFinnigan). Full MS spectra were recorded on the peptides over a 400 to 2000 m/z range by the Orbitrap, followed by five tandem mass (MS/MS) events sequentially generated by LTQ in a data-dependent manner on the first, second, third, and fourth most intense ions selected from the full MS spectrum (at 35% collision energy). Mass spectrometer scan functions and HPLC solvent gradients were controlled by the Xcalibur data system (ThermoFinnigan, San Jose, CA).

Database Search and Interpretation of MS/MS Datasets

Tandem mass spectra were extracted from raw files, and a binary classifier - previously trained on a manually validated data set - was used to remove the low quality MS/MS spectra. The remaining spectra were searched against a *human* protein database downloaded as FASTA-formatted sequences from IPI protein database (database released on January, 2010)[59]. To calculate confidence levels and false positive rates, we used a decoy database containing the reverse sequences of annotated protein sequences appended to the target database, and the SEQUEST algorithm[60] to find the best matching sequences from the combined database.

SEQUEST searches were done using the Integrated Proteomics Pipeline (IP2, Integrated Proteomics Inc., CA) on Intel Xeon X5450 X/3.0 PROC processor clusters running under the Linux operating system. The peptide mass search tolerance was set to 50 ppm. No differential modifications were considered. At least half tryptic status was imposed on the database search, so the search space included all candidate peptides whose theoretical mass fell within the 50 ppm mass tolerance window. The validity of peptide/spectrum matches was assessed in DTASelect2[61] using SEQUEST-defined parameters, the cross-correlation score (XCorr) and normalized difference in cross-correlation scores (DeltaCN). The search results were grouped by charge state (+1, +2, and +3) and tryptic status (fully tryptic, half-tryptic, and non-tryptic), resulting in 9 distinct sub-groups. In each one of the sub-groups, the distribution of XCorr and DeltaCN values for (a) direct and (b) decoy database hits was obtained, and the two subsets were separated by quadratic discriminant analysis. Outlier points in the two distributions (for example, matches with very low Xcorr but very high DeltaCN) were discarded. Full separation of the direct and decoy subsets is not generally possible; therefore, the discriminant score was set such that a false positive rate of 1% was determined based on the number of accepted decoy database peptides. This procedure was independently performed on each data subset, resulting in a false positive rate independent of tryptic status or charge state. In addition, a minimum sequence length of 7 amino acid

residues was required, and each protein on the final list was supported by at least two independent peptide identifications unless otherwise specified. These additional requirements – especially the latter - resulted in the elimination of most decoy database and false positive hits, as these tended to be overwhelmingly present as proteins identified by single peptide matches. After this last filtering step, the false identification rate was reduced to below 1%.

Cell culture and drug treatment

Cell lines were grown at 37°C in an atmosphere of 5% CO_2. Cell lines were obtained from ATCC, unless otherwise stated. Cell lines were identified as negative for mycoplasma contamination. Heat shock was performed at 42°C for 1 h. HEK293T cells were maintained in DMEM medium (Invitrogen) containing 10% (v/v) FBS and 1% (v/v) penicillin/streptomycin. HCT116 cells were cultured in McCoy's 5A (Gibco) containing 10% (v/v) FBS and 1% (v/v) penicillin/streptomycin. A375 cells were cultured in DMEM medium (Invitrogen) containing 10% (v/v) FBS and 1% (v/v) penicillin/streptomycin. 451Lu cells were cultured in TU2% medium containing 80% (v/v) MCDB153, 20% (v/v) Leibovitz's L-15 (Invitrogen), 2% (v/v) FBS, 5 μg/ml bovine insulin, 1.68 mM $CaCl_2$ and 1% (v/v) penicillin/streptomycin. SKMEL239 cells were cultured in RPMI medium containing 10% (v/v) FBS and 1% (v/v) penicillin/streptomycin. 501mel, MM485 and Colo829 were maintained in RPMI 1640 (Gibco) containing 10% (v/v) FBS; SKMEL5 and SKMEL28 in EMEM (Lonza) containing 10% (v/v) FBS; SKMEL24 in MEM (Lonza) containing 10% (v/v) FBS; WC00125, WM3862 and WM39 in tumor media (MCDB153 containing 20% Leibovitz's L-15, 2% fetal bovine serum, 5 μg/ml insulin, 1.68 mM $CaCl_2$). The following drugs were used: MG132 (Peptide Institute), Cycloheximide (Sigma), BIO ((2′*Z*,3′*E*)-6-bromoindirubin- 3′-oxime; GSK3 inhibitor IX; Calbiochem), U0126 (1,4-diamino-2,3-dicyano-1,4-bis[2-aminophenylthio] butadiene; MEK1/2 inhibitor; Cell Signaling), Vemurafenib (PLX4032; $BRAF^{V600E}$ inhibitor; Selleckchem), Trametinib (GSK1120212;MEK1/2 inhibitor; Selleckchem).

Biochemical Methods

For immunoprecipitation experiments, HEK293T were transfected with 10 μg of each vector per 10 cm plate. Two days later, cells were treated with proteasome inhibitor (MG132, 10 μM) for 3 h and cells were lysed in 150 mM NaCl, 50 mM Tris (pH 8.0), 1% NP-40 supplemented with complete protease and phosphatase inhibitors (Roche). HA-tagged proteins were affinity purified from cleared lysates with anti-HA affinity gel (40 ul beads per confluent 10 cm plate; Sigma), washed thoroughly and boiled in SDS loading buffer with 1% β-mercaptoethanol for PAGE separation, followed by western blot analysis. Detection of protein ubiquitylation was carried out as described previously[62]. To quantify protein levels in subcellular compartments, fractionation was performed using subcellular protein fractionation kit for cultured cells (Thermo Scientific). 30 μg of whole cell lysate was loaded per lane, separated on a 4%–12% NuPage Bis-Tris polyacrylamide gel (Invitrogen) and subjected to western blot analysis. The following antibodies were used: FLAG M2 (1:5000, Sigma, F3165), Hsf1 (1:1000, Cell Signaling, 4356), c-Myc (1:1000, Cell Signaling, 9402), Skp1 (1:1000, BD, 610530), Myc-Tag (1:3000, Cell Signaling, 2272), a-Tubulin (1:5000, Santa Cruz, 8035), Lamin B (1:1000, Santa Cruz, 6217), Mcl-1 (1:1000,

Santa Cruz, 819), mTOR (1:1000, Cell Signaling, 2972), SREBP-1 (1:1000, Santa Cruz, 8984), Cyclin E (1:1000, Santa Cruz, 247) and Notch1 (1:1000, Santa Cruz, 6014). Representative blots (Figs 1b, 2, 3a,b, 5a,b,d,e) are shown from three experiments.

Quantitative Real-Time PCR

For mRNA quantification, total RNA was isolated from one million cells for each condition and replicate using the RNeasy Plus Mini Kit (QIAGEN). RNA was quantified by absorbance at A260 nm and 1 μg of total RNA used for cDNA synthesis using Superscript III first strand synthesis kit (Invitrogen). Real time PCR reactions were carried out using SYBR Green Master Mix (Roche) and run with a Lightcycler 480 II (Roche). The following primer sequences were used for cDNA quantification: *HSF1* for CCGTGTCCTGTGGTTTGGTT, rev CTGTCTTGTCCGTCCATCCA; *HSPA6* for AGCAGTTGTGGCACTCAAG, rev TCACAGCTGACTTATCACGAAG; *HSPD1* for ACGGCTTGCAAAACTTTCAG, rev TTAAGGGCATCTGTAACTCTGTC; *HSP90AB1* for AGCAGCAGTAGTGGGACCAT, rev TAGAAGTGGCAGCAATCACG; *DNAJB1* for GAGATCTTCGACCGCTACG, rev CCATGGAATGTGTAGCTGAAAG; *HSPE1* for ACACTAGAGCAGAGTACGAGTC, rev CAGCACTCCTTTCAACCAATAC; *HSPH1* for CACCAGAAAACCCAGACACT, rev GGGAGACTGTGAGGTTTGTT; *CCNE1* for TCTTTGTCAGGTGTGGGGA, rev GAAATGGCCAAAATCGACAG; *ADAM17* for TCTGAGAGCAAAGAATCAAGC, rev TCCTATTCCTGACCAGCGTG; *ADAM22* for CAGTCTTGCCTCCATGTTCA, rev GCCTTTGGAACGTCATTCAT; *HMGB1* for AGGATCTCCTTTGCCCATGT, rev TGAGCTCCATAGAGACAGCG; *ITGB3BP* for TTCTCAACTTTTGATAGCAACATCA, rev GACTCCCGACTTGACACGAT; *MTHFD2* for CACTCTTCTACCTCCTGCCG, rev TTCGCCCTTTCCACCTC.

Immunohistochemistry

Immunohistochemistry was performed on Formalin-Fixed, Paraffin Embedded (FFPE) slides using the Avidin/Biotinylated enzyme system (VECTASTAIN ABC, Vector Laboratories). Heat induced epitope retrieval was performed using a pressure cooker with Tris-EDTA Buffer. Samples were provided by the Biospecimen Core of the NYU IMCG. The number of melanoma samples was selected based on the homogeneity of HSF1 staining in nevi, primary and metastatic samples. No statistical method was used to predetermine sample size. No samples were excluded or randomized. The study protocol was approved by the NYU Institutional Review Committee (IRB). All NYU patients signed informed consent. The anti-HSF1 antibody (1:10000, Thermo Scientific, RT-629-PABX). The anti-FBXW7 antibody (1:2000, Abcam, 109617). The slides were reviewed and scored by IMCG pathologist (FD) according to the intensity (0-2) of the staining as well as distribution (focal <50%, diffuse ≥50%). The IMCG pathologist was blinded while scoring the samples. In addition, rabbit anti-human Ki67, clone Sp6 (1:400; Thermoscientific; MA1-90584), mouse anti-human Melan-A, clone A103 (1:75; Dako; M7196) and mouse anti-human Tyrosinase, clone T311 (1:100; Biocare Medical; 155) were used.

FBXW7 Transient Knockdown

For transient knockdown of *FBXW7*, human melanoma cell lines were transfected with scrambled siRNA (D-001810-10, ON-TARGETplus Non-targeting Pool) or *FBXW7*-specific siRNA (L-004264-00) (ON-TARGETplus SMARTpool, Dharmacon, Lafayette, CO, USA) using JetPrime (Polyplus transfection, France). Seventy-two hours after siRNA transfection, cells were collected and total RNA was extracted for further analyses.

In vitro Invasion Assay

Cell migration was measured using transwell inserts (8 μm pores, BD Falcon). 451Lu cells (30.000 cells per insert) were suspended in serum-free medium over a Matrigel coating (Becton Dickinson), and medium supplemented with serum was used as chemoattractant. Cells that migrated after 12 hours were fixed in glutaraldehyde 0.1% solution, stained with 0.5% crystal violet, and counted in ten different fields using an inverted microscope. For each independent experiment, four replicates per condition were run. The average of cell counts from four inserts per condition was used for plotting results.

In vivo Metastasis Assay

451Lu cells transduced with sh*Luc* or sh*FBXW7* lentiviruses were resuspended in growth media at a concentration of 2x 10^6 cells/150 uL, aliquoted into Eppendorf tubes (150 uL) and maintained on ice until injection. Immediately prior to injection, cell aliquots were mixed with 150 uL Matrigel (Becton Dickinson). Cell/Matrigel (1:1) suspensions were injected subcutaneously in the right flank of NOD/Shi-*scid*/IL-2Rγ^{null} (NOG) 8 week old female mice (sh*LUC* n=8; sh*FBXW7* n=7). No statistic method was used to predetermine sample size. The experiments were not randomized. No samples were excluded from the analysis. In vivo experiments were performed in compliance with a referenced protocol (120405-03) approved by the Institutional Animal Care and Use Committee (IACUC). When tumors were palpable (15 days), length and width measurements were made with calipers 3 times weekly until the animals were sacrificed. Tumor volume was calculated by the following formula: a^2*b/2, where a is the width and b is the length. 40 days after subcutaneous injection, all animals were sacrificed to assess tumor mass and quantify lung metastasis. Tumors were extracted, weighed, formalin-fixed and paraffin-embedded. Lungs, liver, spleen, and kidney were removed for analysis of metastasis. Ventral and dorsal macroscopic images of metastasis-bearing lungs were taken with a fluorescent dissecting microscope equipped with a black and white camera. Pictures of the same lung were stitched and macroscopic metastases were quantified by counting lesions in both sides of lung per mouse. Representative images from tumors from 5 mice per condition are included. Data were plotted using GraphPad PRISM and significance determined by unpaired *t* test.

Detection of Cell Death

Cells were transduced with scrambled and shRNA targeting HSF1 as indicated, collected and directly stained by addition of Pacific Blue™-Annexin V (Biolegend) and 1 μg/mL propidium iodide (PI) 10 mM HEPES/NaOH (pH 7.4), 140 mM NaCl and 2.5 mM $CaCl_2$ for 20 by flow cytometry (LSRII; Becton Dickinson) and the population with Annexin-V

positive and PI negative staining was considered apoptotic. Representative images (5f) are shown from three experiments.

Survival Assays

Relative cell growth and survival was measured in 96-well microplate using the resazurin cell viability kit (Cell Signaling). Cells were plated at low density (~3000 cells/well) and exposed for 3 days to the indicated concentrations of proteotoxic drugs.

Statistics

Data are presented as the mean ± s.d. and were plotted using GraphPad PRISM. Significance was determined using an unpaired Student's t-test. For multiple comparisons, we used two-way ANOVA, corrected by the post-hoc Bonferroni test.

Chromatin Immunoprecipitation

For ChIP-Seq, 5×10^6 HCT116 cells were used for each immunoprecipitation. 5 μg of HSF1 antibody (Cell Signaling, 4356) was used per immunoprecipitation. ChIP and ChIP-Seq experiments were performed as described previously[63].

RNA-Sequencing Library Preparation

Total RNA was isolated from 1 million HCT116 cells using RNeasy Plus kit (Qiagen). Ribosomal RNA was depleted using RiboZero magnetic kit (Epicenter) according to manufacturer's protocol. cDNA preparation and strand-specific library construction was performed using the dUTP method as described previously[64]. Libraries were sequenced on the Illumina HiSeq 2000 using 50bp single end reads.

Data Sources and Computational Tools

Human assembly version hg19/GRCh37 and ENSEMBL annotations release 69 were used for the RNA-sequencing, ChIP-sequencing and data integration analyses. Bowtie[65] version 0.12.7 was used for alignment of sequenced reads. RNA-sequencing data analysis was performed using the DEGseq[66]. MACS[67] version 1.4.2 was used for ChIP-sequencing peak discovery. GenomicTools[68] version 2.7.2 was used for performing genomic interval mathematical operations, genomic interval annotations and ChIP-seq profile construction.

HSF1 Peak Identification

HSF1 ChIP-sequenced reads were aligned using bowtie (with default parameters, except for –m 1 so as to report only unique alignments) on human assembly version hg19. Peak discovery was performed with MACS using default parameters except for using a fragment size of 270bp estimated by Agilent 2100 Bioanalyzer. Sonicated input was used as a control for peak discovery. HSF1 peaks were characterized according to their genome-wide distribution into: (a) 1kb TSS-flanking regions of transcript isoforms, (b) gene body regions (excluding any overlapping regions with (a)), and (c) upstream regions of minimum 10kb and up to a maximum of 100kb (excluding any overlapping regions with (a) or (b)).

RNA-Sequencing Analysis

Differential gene expression analysis was performed for each matched recovery versus heat-shock pairs, separately in each biological replicate and cell line (WT or KO). Analysis was performed using DEGseq[66]. Input to DEGseq (i.e. gene RNA-seq counts) were computed using GenomicTools[68]. P-value cutoff (adjusted for multiple hypothesis testing) for differential expression was set at 1e-5, and genes presented in the heatmap have absolute log2 fold-change greater than 0.5 and FPKM value greater than 2.0 (in heat shock, recovery or both). To enforce more stringent criteria for significant differential expression, we ran DEGseq on each matched heat shock-recovery pair of biological replicates, and filtered out genes with inconsistent changes between replicates. The genes shown in the heatmap are the common HSF1 heat-shock response targets identified by ChIP-Seq analysis in HCT116 WT and *FBXW7* KO cells and are significantly differentially expressed in recovery versus heat shock in at least one of the cell lines.

HSF1 mRNA signature and correlation analysis with *FBXW7* expression

mRNA expression (level 3 normalized RNAseq results) of 325 Skin Cutaneous Melanoma (SKCM) cases were obtained from the Cancer Genome Atlas (TCGA) Data Portal (http://tcga-data.nci.nih.gov). HSF1 mRNA signature was defined as mRNA expressions that were significantly correlated with HSF1 expression (NM_005526) with Spearman Correlation Coefficient > 0.3 and FDR < 5% in TCGA samples. Among them, mRNAs with positive correlations were defined as the positive signature, while mRNAs with negative correlations were defined as the negative signature. Spearman correlation coefficient was used to examine the correlation between FBXW7 (NM_033632) expression and first Principal Component (PC1) of HSF1 positive signature and PC1 of HSF1 negative signature respectively.

Supplementary Material

Refer to Web version on PubMed Central for supplementary material.

Acknowledgments

We would like to thank the members of the Aifantis laboratory for helpful discussions. Dr. B. Vogelstein for the HCT116 cell lines. Drs. M. Pagano and L. Busino for helpful discussions and for plasmids. The Aifantis Lab is supported by the National Institutes of Health (1R01CA169784-02, 1R01CA133379-06, 1R01CA105129-08, 1R01CA149655-04, 5R01CA173636-03, 1R24OD018339-01), the William Lawrence and Blanche Hughes Foundation, The Leukemia & Lymphoma Society (TRP#6340-11, LLS#6373-13), The Chemotherapy Foundation, The V Foundation for Cancer Research, the Alex's Lemonade Stand Foundation for Childhood Cancer and the St. Baldrick's Cancer Research Foundation. FBXW7 work has also been supported by a NY STEM grant (CO28130). The Hernando Lab is supported by the NIH/NCI (1R01CA155234, 1R01CA163891-01A1) and the Department of Defense (DOD) Collaborative Award (CA093471). B.A.O is supported by Deutsche Jose Carreras Leukaemie Stiftung. N.K is supported by a European Molecular Biology Organization (EMBO) Long Term Fellowship and a Human Frontiers Science Program (HFSP) Long Term Fellowship. I.A. is a Howard Hughes Medical Institute Early Career Scientist.

REFERENCES

1. Pelham HR. A regulatory upstream promoter element in the Drosophila hsp 70 heat-shock gene. Cell. 1982; 30:517–528. [PubMed: 6814763]

2. Westerheide SD, Morimoto RI. Heat shock response modulators as therapeutic tools for diseases of protein conformation. The Journal of biological chemistry. 2005; 280:33097–33100. [PubMed: 16076838]

3. Whitesell L, Lindquist SL. HSP90 and the chaperoning of cancer. Nature reviews. Cancer. 2005; 5:761–772. [PubMed: 16175177]

4. Jolly C, Morimoto RI. Role of the heat shock response and molecular chaperones in oncogenesis and cell death. Journal of the National Cancer Institute. 2000; 92:1564–1572. [PubMed: 11018092]

5. Jin X, Moskophidis D, Mivechi NF. Heat shock transcription factor 1 is a key determinant of HCC development by regulating hepatic steatosis and metabolic syndrome. Cell metabolism. 2011; 14:91–103. [PubMed: 21723507]

6. Min JN, Huang L, Zimonjic DB, Moskophidis D, Mivechi NF. Selective suppression of lymphomas by functional loss of Hsf1 in a p53-deficient mouse model for spontaneous tumors. Oncogene. 2007; 26:5086–5097. [PubMed: 17310987]

7. Dai C, Whitesell L, Rogers AB, Lindquist S. Heat shock factor 1 is a powerful multifaceted modifier of carcinogenesis. Cell. 2007; 130:1005–1018. [PubMed: 17889646]

8. Dai C, et al. Loss of tumor suppressor NF1 activates HSF1 to promote carcinogenesis. The Journal of clinical investigation. 2012; 122:3742–3754. [PubMed: 22945628]

9. Luo J, Solimini NL, Elledge SJ. Principles of cancer therapy: oncogene and non-oncogene addiction. Cell. 2009; 136:823–837. [PubMed: 19269363]

10. Meng L, Gabai VL, Sherman MY. Heat-shock transcription factor HSF1 has a critical role in human epidermal growth factor receptor-2-induced cellular transformation and tumorigenesis. Oncogene. 2010; 29:5204–5213. [PubMed: 20622894]

11. Santagata S, et al. Using the heat-shock response to discover anticancer compounds that target protein homeostasis. ACS chemical biology. 2012; 7:340–349. [PubMed: 22050377]

12. Solimini NL, Luo J, Elledge SJ. Non-oncogene addiction and the stress phenotype of cancer cells. Cell. 2007; 130:986–988. [PubMed: 17889643]

13. Zhao Y, et al. Overcoming trastuzumab resistance in breast cancer by targeting dysregulated glucose metabolism. Cancer research. 2011; 71:4585–4597. [PubMed: 21498634]

14. Scherz-Shouval R, et al. The reprogramming of tumor stroma by HSF1 is a potent enabler of malignancy. Cell. 2014; 158:564–578. [PubMed: 25083868]

15. Mendillo ML, et al. HSF1 drives a transcriptional program distinct from heat shock to support highly malignant human cancers. Cell. 2012; 150:549–562. [PubMed: 22863008]

16. Santagata S, et al. Tight coordination of protein translation and HSF1 activation supports the anabolic malignant state. Science. 2013; 341:1238303. [PubMed: 23869022]

17. Anckar J, Sistonen L. Regulation of HSF1 function in the heat stress response: implications in aging and disease. Annual review of biochemistry. 2011; 80:1089–1115.

18. Hu Y, Mivechi NF. Promotion of heat shock factor Hsf1 degradation via adaptor protein filamin A-interacting protein 1-like (FILIP-1L). The Journal of biological chemistry. 2011; 286:31397–31408. [PubMed: 21784850]

19. Akerfelt M, Morimoto RI, Sistonen L. Heat shock factors: integrators of cell stress, development and lifespan. Nature reviews. Molecular cell biology. 2010; 11:545–555. [PubMed: 20628411]

20. Skaar JR, Pagan JK, Pagano M. Mechanisms and function of substrate recruitment by F-box proteins. Nature reviews. Molecular cell biology. 2013; 14:369–381. [PubMed: 23657496]

21. Busino L, et al. Fbxw7alpha- and GSK3-mediated degradation of p100 is a pro-survival mechanism in multiple myeloma. Nat Cell Biol. 2012; 14:375–385. [PubMed: 22388891]

22. Davis MA, et al. The SCF-Fbw7 ubiquitin ligase degrades MED13 and MED13L and regulates CDK8 module association with Mediator. Genes & development. 2013; 27:151–156. [PubMed: 23322298]

23. Davis RJ, Welcker M, Clurman BE. Tumor Suppression by the Fbw7 Ubiquitin Ligase: Mechanisms and Opportunities. Cancer cell. 2014; 26:455–464. [PubMed: 25314076]

24. Oberg C, et al. The Notch intracellular domain is ubiquitinated and negatively regulated by the mammalian Sel-10 homolog. The Journal of biological chemistry. 2001; 276:35847–35853. [PubMed: 11461910]

25. Strohmaier H, et al. Human F-box protein hCdc4 targets cyclin E for proteolysis and is mutated in a breast cancer cell line. Nature. 2001; 413:316–322. [PubMed: 11565034]
26. Wang Z, Liu P, Inuzuka H, Wei W. Roles of F-box proteins in cancer. Nature reviews. Cancer. 2014; 14:233–247. [PubMed: 24658274]
27. Welcker M, et al. The Fbw7 tumor suppressor regulates glycogen synthase kinase 3 phosphorylation-dependent c-Myc protein degradation. Proceedings of the National Academy of Sciences of the United States of America. 2004; 101:9085–9090. [PubMed: 15150404]
28. Inuzuka H, et al. SCF(FBW7) regulates cellular apoptosis by targeting MCL1 for ubiquitylation and destruction. Nature. 2011; 471:104–109. [PubMed: 21368833]
29. King B, et al. The ubiquitin ligase FBXW7 modulates leukemia-initiating cell activity by regulating MYC stability. Cell. 2013; 153:1552–1566. [PubMed: 23791182]
30. Akhoondi S, et al. FBXW7/hCDC4 is a general tumor suppressor in human cancer. Cancer research. 2007; 67:9006–9012. [PubMed: 17909001]
31. He B, Meng YH, Mivechi NF. Glycogen synthase kinase 3beta and extracellular signal-regulated kinase inactivate heat shock transcription factor 1 by facilitating the disappearance of transcriptionally active granules after heat shock. Molecular and cellular biology. 1998; 18:6624–6633. [PubMed: 9774677]
32. Hietakangas V, et al. Phosphorylation of serine 303 is a prerequisite for the stress-inducible SUMO modification of heat shock factor 1. Molecular and cellular biology. 2003; 23:2953–2968. [PubMed: 12665592]
33. Kline MP, Morimoto RI. Repression of the heat shock factor 1 transcriptional activation domain is modulated by constitutive phosphorylation. Molecular and cellular biology. 1997; 17:2107–2115. [PubMed: 9121459]
34. Knauf U, Newton EM, Kyriakis J, Kingston RE. Repression of human heat shock factor 1 activity at control temperature by phosphorylation. Genes & development. 1996; 10:2782–2793. [PubMed: 8946918]
35. Wang X, Grammatikakis N, Siganou A, Stevenson MA, Calderwood SK. Interactions between extracellular signal-regulated protein kinase 1, 14-3-3epsilon, and heat shock factor 1 during stress. The Journal of biological chemistry. 2004; 279:49460–49469. [PubMed: 15364926]
36. Xavier IJ, et al. Glycogen synthase kinase 3beta negatively regulates both DNA-binding and transcriptional activities of heat shock factor 1. The Journal of biological chemistry. 2000; 275:29147–29152. [PubMed: 10856293]
37. Chu B, Soncin F, Price BD, Stevenson MA, Calderwood SK. Sequential phosphorylation by mitogen-activated protein kinase and glycogen synthase kinase 3 represses transcriptional activation by heat shock factor-1. The Journal of biological chemistry. 1996; 271:30847–30857. [PubMed: 8940068]
38. Rajagopalan H, et al. Inactivation of hCDC4 can cause chromosomal instability. Nature. 2004; 428:77–81. [PubMed: 14999283]
39. Santagata S, et al. High levels of nuclear heat-shock factor 1 (HSF1) are associated with poor prognosis in breast cancer. Proceedings of the National Academy of Sciences of the United States of America. 2011; 108:18378–18383. [PubMed: 22042860]
40. Thompson BJ, et al. Control of hematopoietic stem cell quiescence by the E3 ubiquitin ligase Fbw7. The Journal of experimental medicine. 2008; 205:1395–1408. [PubMed: 18474632]
41. Cheng Y, Chen G, Martinka M, Ho V, Li G. Prognostic significance of Fbw7 in human melanoma and its role in cell migration. J Invest Dermatol. 2013; 133:1794–1802. [PubMed: 23381582]
42. Holderfield M, Deuker MM, McCormick F, McMahon M. Targeting RAF kinases for cancer therapy: BRAF-mutated melanoma and beyond. Nature reviews. Cancer. 2014; 14:455–467. [PubMed: 24957944]
43. Scott KL, et al. Proinvasion metastasis drivers in early-stage melanoma are oncogenes. Cancer cell. 2011; 20:92–103. [PubMed: 21741599]
44. Kabbarah O, et al. Integrative genome comparison of primary and metastatic melanomas. PloS one. 2010; 5:e10770. [PubMed: 20520718]
45. Olive V, et al. A component of the mir-17-92 polycistronic oncomir promotes oncogene-dependent apoptosis. eLife. 2013; 2:e00822. [PubMed: 24137534]

46. Wang L, Ye X, Liu Y, Wei W, Wang Z. Aberrant regulation of FBW7 in cancer. Oncotarget. 2014; 5:2000–2015. [PubMed: 24899581]
47. Abravaya K, Myers MP, Murphy SP, Morimoto RI. The human heat shock protein hsp70 interacts with HSF, the transcription factor that regulates heat shock gene expression. Genes & development. 1992; 6:1153–1164. [PubMed: 1628823]
48. Satyal SH, Chen D, Fox SG, Kramer JM, Morimoto RI. Negative regulation of the heat shock transcriptional response by HSBP1. Genes & development. 1998; 12:1962–1974. [PubMed: 9649501]
49. Shi Y, Mosser DD, Morimoto RI. Molecular chaperones as HSF1-specific transcriptional repressors. Genes & development. 1998; 12:654–666. [PubMed: 9499401]
50. Westerheide SD, Anckar J, Stevens SM Jr. Sistonen L, Morimoto RI. Stress-inducible regulation of heat shock factor 1 by the deacetylase SIRT1. Science. 2009; 323:1063–1066. [PubMed: 19229036]
51. Raychaudhuri S, et al. Interplay of Acetyltransferase EP300 and the Proteasome System in Regulating Heat Shock Transcription Factor 1. Cell. 2014; 156:975–985. [PubMed: 24581496]
52. Whitesell L, Lindquist S. Inhibiting the transcription factor HSF1 as an anticancer strategy. Expert opinion on therapeutic targets. 2009; 13:469–478. [PubMed: 19335068]
53. Wang Y, et al. Rapamycin inhibits FBXW7 loss-induced epithelial-mesenchymal transition and cancer stem cell-like characteristics in colorectal cancer cells. Biochemical and biophysical research communications. 2013; 434:352–356. [PubMed: 23558291]
54. Hagedorn M, et al. FBXW7/hCDC4 controls glioma cell proliferation in vitro and is a prognostic marker for survival in glioblastoma patients. Cell division. 2007; 2:9. [PubMed: 17326833]
55. Iwatsuki M, et al. Loss of FBXW7, a cell cycle regulating gene, in colorectal cancer: clinical significance. International journal of cancer. Journal international du cancer. 2010; 126:1828–1837. [PubMed: 19739118]
56. Yokobori T, et al. p53-Altered FBXW7 expression determines poor prognosis in gastric cancer cases. Cancer research. 2009; 69:3788–3794. [PubMed: 19366810]
57. Hao B, Oehlmann S, Sowa ME, Harper JW, Pavletich NP. Structure of a Fbw7-Skp1-cyclin E complex: multisite-phosphorylated substrate recognition by SCF ubiquitin ligases. Molecular cell. 2007; 26:131–143. [PubMed: 17434132]
58. Riker AI, et al. The gene expression profiles of primary and metastatic melanoma yields a transition point of tumor progression and metastasis. BMC medical genomics. 2008; 1:13. [PubMed: 18442402]
59. Kersey PJ, et al. The International Protein Index: an integrated database for proteomics experiments. Proteomics. 2004; 4:1985–1988. [PubMed: 15221759]
60. Yates JR 3rd, Eng JK, McCormack AL, Schieltz D. Method to correlate tandem mass spectra of modified peptides to amino acid sequences in the protein database. Analytical chemistry. 1995; 67:1426–1436. [PubMed: 7741214]
61. Tabb DL, McDonald WH, Yates JR 3rd. DTASelect and Contrast: tools for assembling and comparing protein identifications from shotgun proteomics. Journal of proteome research. 2002; 1:21–26. [PubMed: 12643522]
62. Choo YS, Zhang Z. Detection of protein ubiquitination. Journal of visualized experiments: JoVE. 2009
63. Ntziachristos P, et al. Genetic inactivation of the polycomb repressive complex 2 in T cell acute lymphoblastic leukemia. Nature medicine. 2012; 18:298301.
64. Zhong S, et al. High-throughput illumina strand-specific RNA sequencing library preparation. Cold Spring Harb Protoc. 2011; 2011:940–949. [PubMed: 21807852]
65. Langmead B, Trapnell C, Pop M, Salzberg SL. Ultrafast and memory-efficient alignment of short DNA sequences to the human genome. Genome biology. 2009; 10:R25. [PubMed: 19261174]
66. Wang L, Feng Z, Wang X, Wang X, Zhang X. DEGseq: an R package for identifying differentially expressed genes from RNA-seq data. Bioinformatics. 2010; 26:136–138. [PubMed: 19855105]
67. Zhang Y, et al. Model-based analysis of ChIP-Seq (MACS). Genome biology. 2008; 9:R137. [PubMed: 18798982]

68. Tsirigos A, Haiminen N, Bilal E, Utro F. GenomicTools: a computational platform for developing high-throughput analytics in genomics. Bioinformatics. 2012; 28:282–283. [PubMed: 22113082]

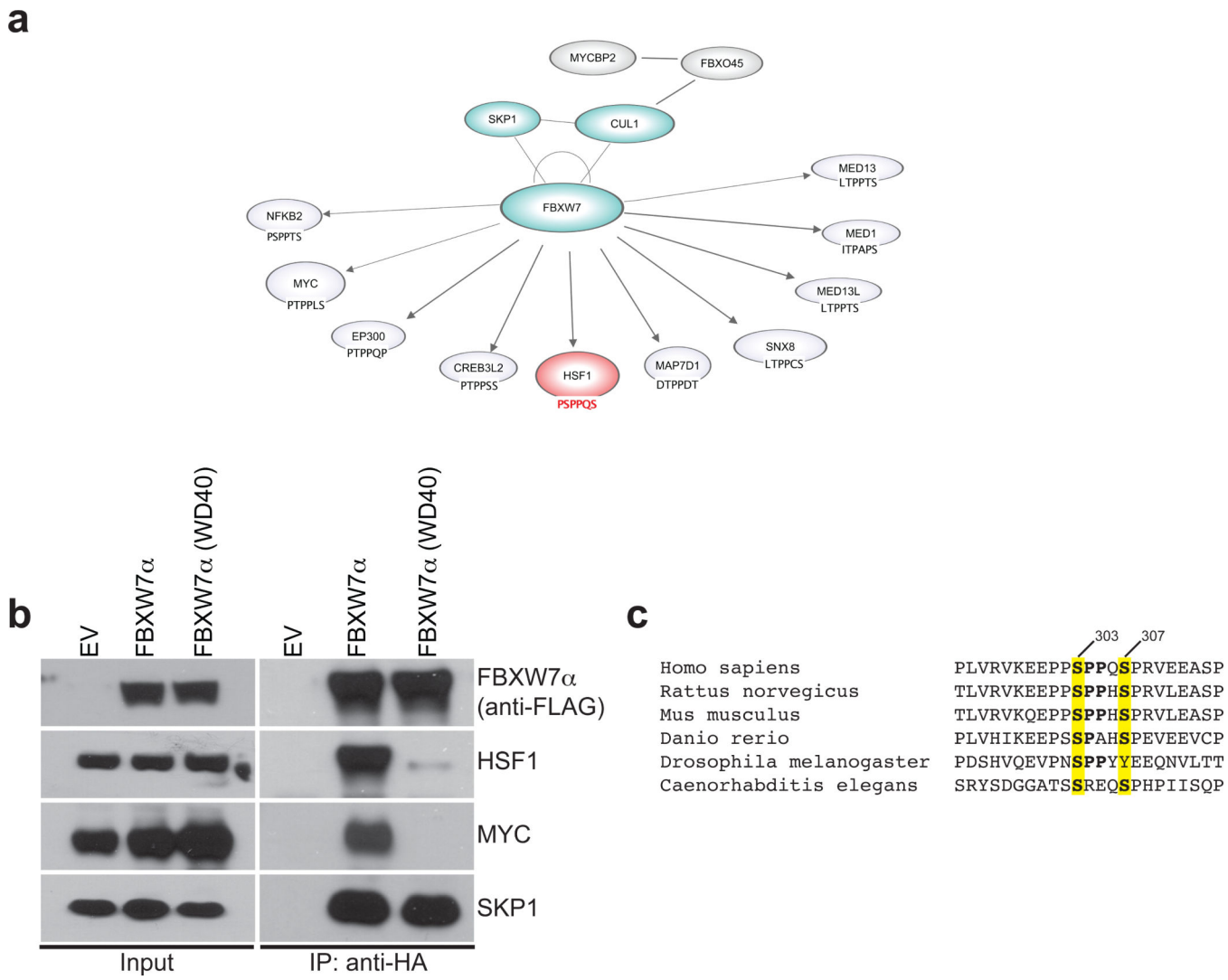

Figure 1. HSF1 is a substrate of the FBXW7α ubiquitin ligase

(**a**) Network of FBXW7α-interacting partners. Serial immunoprecipitation experiments from HEK293 cells coupled to mass-spectrometry based analysis revealed a large number of known substrates (NFKB2, MYC, MED13L, MED13), already characterized members of the Cullin 1 complex (SKP1, CUL1) and putative interactors (MED1, HSF1). The FBXW7 degrons on various substrates are indicated. (**b**) FBXW7α binds to HSF1 through specific residues in the WD40 domain. HEK293T cells were transfected with constructs encoding FLAG tagged HSF1, and FLAG-HA tagged empty vector (EV), or FLAG-HA tagged FBXW7α or FLAG-HA tagged FBXW7α (WD40), a substrate binding mutant, in which three residues within one of the seven WD40 repeats of *FBXW7*α have been mutated[57]. HA-tagged FBXW7α was immunoprecipitated (IP) from cell extracts with anti-HA resin, followed by immunoblotting as indicated. The left panel shows inputs. (**c**) Alignment of the human HSF1 protein region containing the putative degron with HSF1 from various organisms. Conserved phospho-amino acids (amino acids 303 and 307 in human sequence) are highlighted. Uncropped blots are shown in Supplementary Fig. 8.

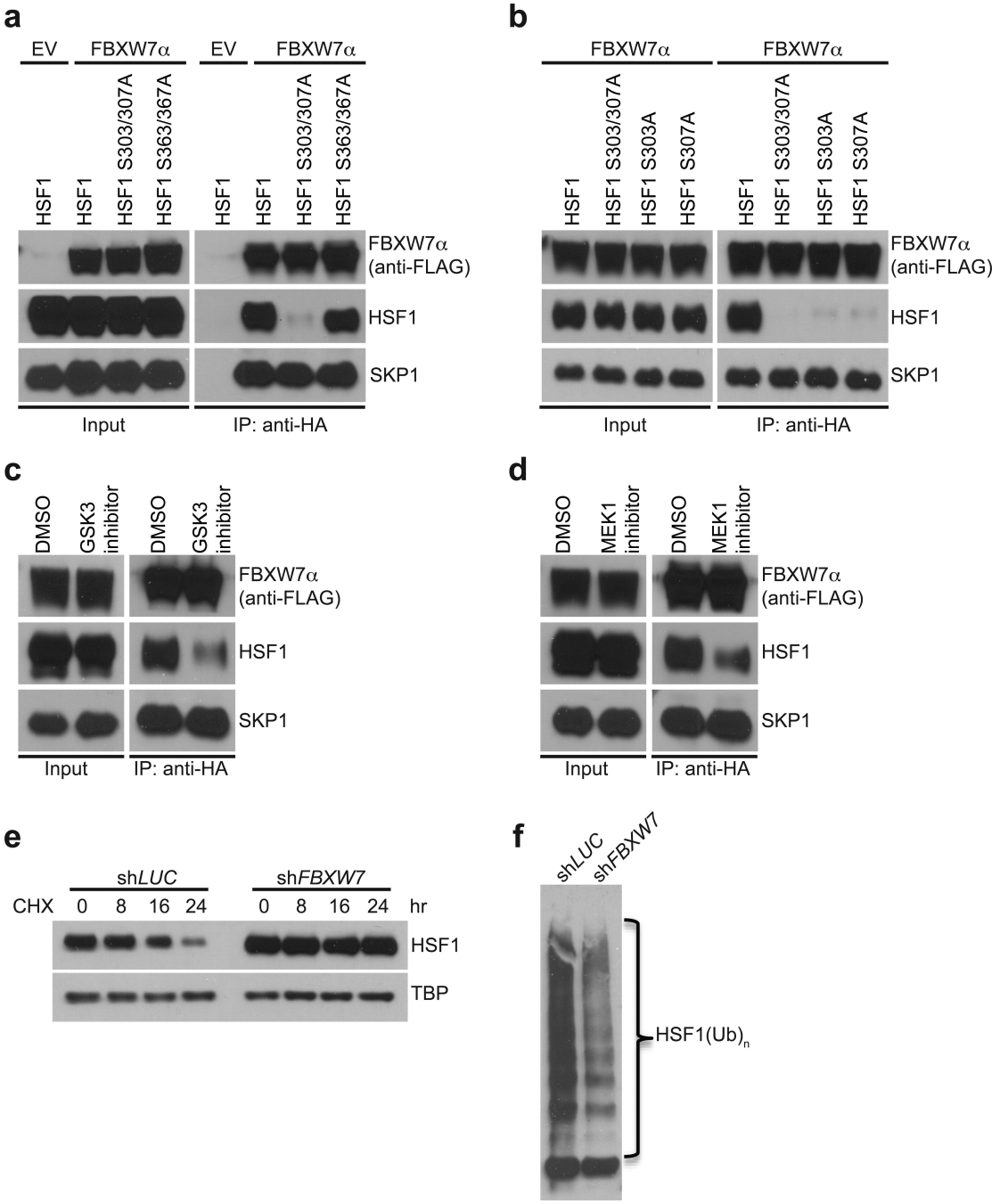

Figure 2. HSF1 interacts with FBXW7α through a conserved degron sequence phosphorylated by GSK3β and ERK1

(**a**) HSF1 binds FBXW7α through a conserved degron. HEK293T cells were transfected with FLAG-HA tagged FBXW7α and constructs encoding FLAG tagged HSF1 or HSF1(Ser303/307Ala) or HSF1(Ser363/367Ala). HA-tagged FBXW7α was immunoprecipitated (IP) from cell extracts with anti-HA resin, followed by immunoblotting as indicated. The left panel shows inputs. (**b**) Both Ser303 and Ser307 in HSF1 are required for the interaction with FBXW7α. HEK293T cells were transfected with FLAG-HA tagged FBXW7α and constructs encoding FLAG tagged HSF1 or HSF1(Ser303/307Ala) or

HSF1(Ser303Ala) or HSF1(Ser307Ala). HA-tagged FBXW7α was immunoprecipitated (IP) from cell extracts with anti-HA resin, followed by immunoblotting as indicated. (**c**) Interaction between HSF1 and FBXW7α depends on GSK3β activity. HEK293T cells were transfected with constructs encoding FLAG tagged HSF1 and FLAG-HA tagged FBXW7α. Cells were treated with GSK3i IX (10 μM for 10 h) or DMSO. HA-tagged FBXW7α was immunoprecipitated (IP) from cell extracts with anti-HA resin, followed by immunoblotting as indicated. (**d**) Interaction between HSF1 and FBXW7α depends on ERK1 activity. HEK293T cells were transfected with constructs encoding FLAG tagged HSF1 and FLAG-HA tagged FBXW7α. Cells were treated with MEK1 inhibitor U0126 (10 μM for 2 h) or DMSO. HA-tagged FBXW7α was immunoprecipitated (IP) from cell extracts with anti-HA resin, followed by immunoblotting as indicated. (**e**) FBXW7α controls the half-life of nuclear HSF1. HEK293T cells were infected with the indicated shRNA-encoding lentiviruses. Cells were treated with 2 μg/ml cycloheximide for the indicated length of time. Nuclear fractions were analyzed by immunoblotting as indicated. TATA-binding protein (TBP) was used as loading control. (**f**) *FBXW7*α depletion abolishes HSF1 ubiquitylation *in vivo*. HEK293T cells were transfected with constructs encoding FLAG tagged HSF1 and Histidine-Myc tagged ubiquitin and infected with the indicated shRNA-encoding lentiviruses. Cells were heat shocked at 42°C for 1 h to induce ubiquitylation. Histidine tagged proteins were immunoprecipitated from whole cell extracts with nickel (Ni)-NTA beads, followed by immunoblotting for HSF1. Uncropped blots are shown in Supplementary Fig. 8.

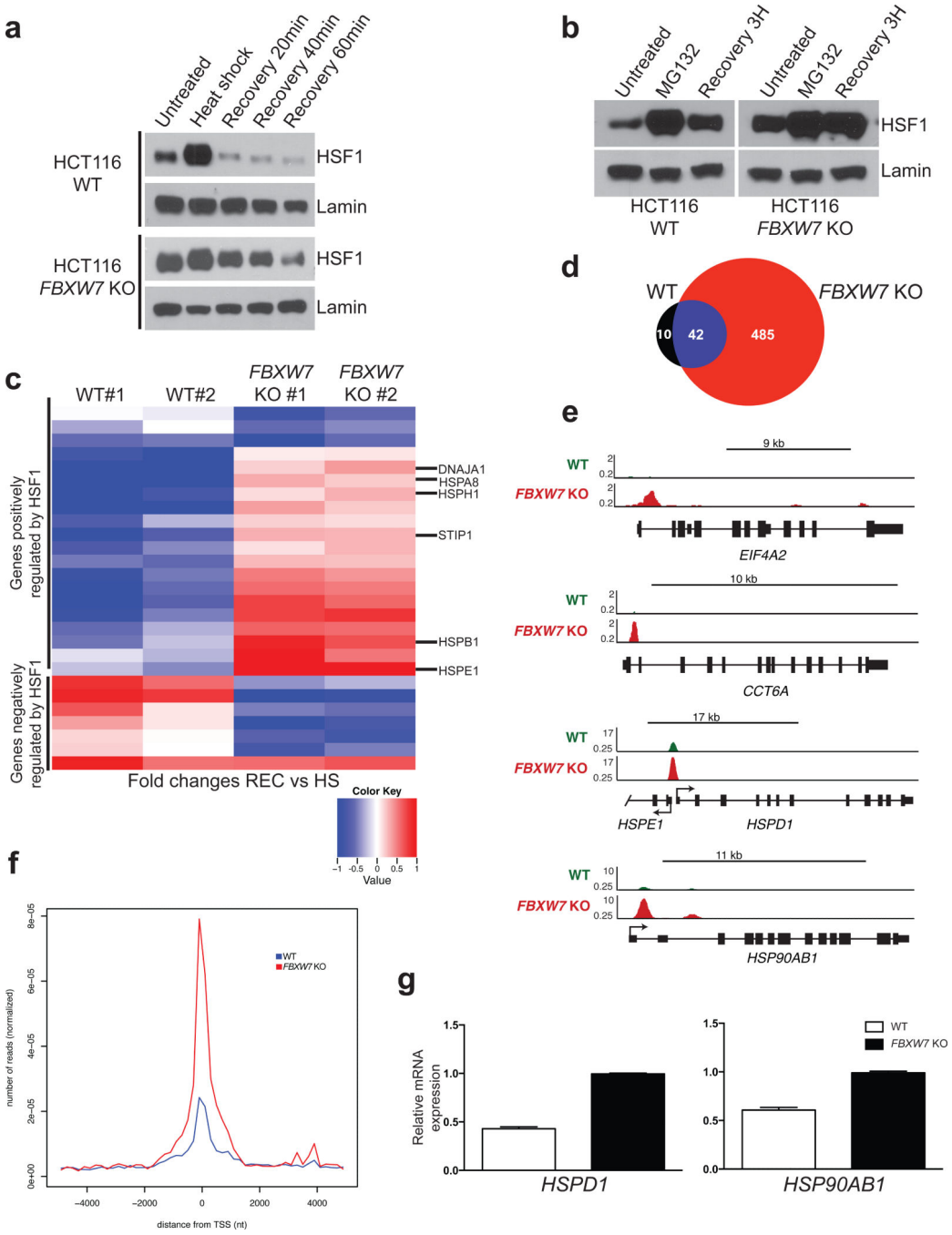

Figure 3. *FBXW7* deficiency results in nuclear HSF1 accumulation and prolonged heat-shock response upon exposure to exogenous stress

(**a**) Loss of *FBXW7* results in accumulation of nuclear HSF1 during recovery from heat shock. HCT116 WT and *FBXW7* KO cells were heat shocked (42°C for 1 h) following recovery for the indicated time. Nuclear fractions were analyzed by immunoblotting as indicated. (**b**) Loss of *FBXW7* results in accumulation of nuclear HSF1 during recovery from proteotoxic stress. HCT116 WT and *FBXW7* KO cells were treated with MG132 (1 μM for 10 h) following recovery for 3 h. Nuclear fractions were analyzed by immunoblotting as

indicated. (**c**) *FBXW7* KO cells show defective attenuation of the heat-shock response pathway. Heat maps showing fold changes in expression of HSF1 targets comparing recovery (37°C for 2 h) to heat shock (42°C for 1 h) as determined by high-throughput RNA-Seq. The common targets of HSF1 in HCT116 WT and *FBXW7* KO cells after heat shock, as revealed by ChIP-Seq analysis, are displayed on the heat map. Well-characterized genes, positively regulated by HSF1, are indicated. Each column represents a biological replicate. (**d**) Overlap of genes bound by HSF1 in HCT116 WT and *FBXW7* KO cells, under basal conditions. (**e**) Representative ChIP-Seq tracks for common gene loci between WT and KO (*HSPD1*/*E1*, *HSP90AB1*) and unique for KO gene loci (EIF4A2, CCT6A). The scale corresponds to RPM. (**f**) Read density profile around TSS's of common HSF1 targets in WT and *FBXW7* KO cells. (**g**) *HSPD1* and *HSP90AB1* mRNA expression in HCT116 WT and *FBXW7* KO cells, under basal conditions ($P<0.001$ for WT versus KO; unpaired *t*-test). Error bars indicate mean ± SD, and n=3 independent experiments. Uncropped blots are shown in Supplementary Fig. 8.

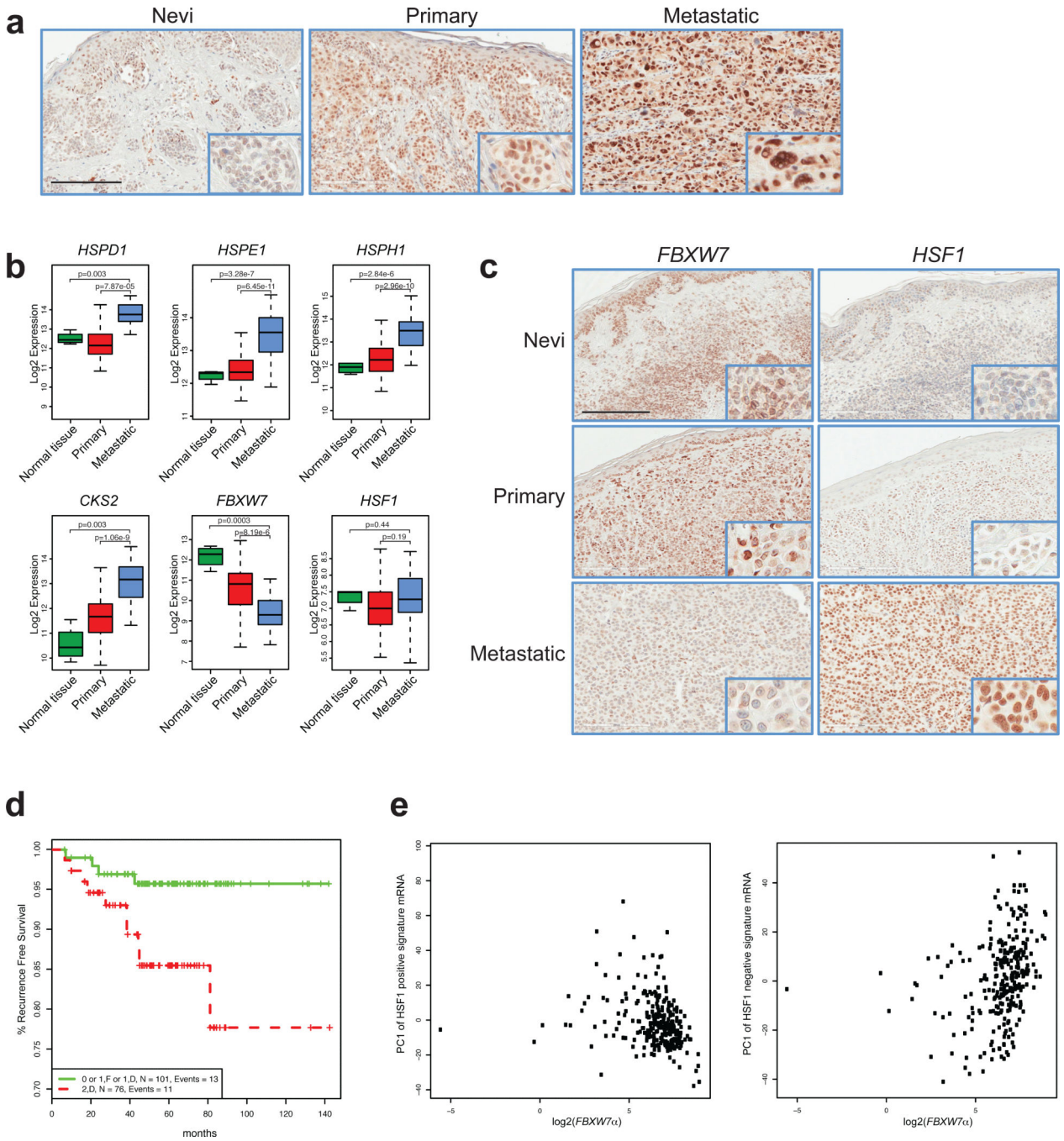

Figure 4. HSF1 protein levels and HSF1 targets expression are associated with metastasis and disease progression in melanoma

(**a**) IHC staining with anti-HSF1 antibody of the indicated tissue types (dysplastic nevi n=48, primary n=39 and metastatic n=45; $P<0.001$ for metastatic versus primary or nevi; unpaired *t*-test; scale bar, 200 μm). (**b**) Box plots showing expression of HSF1 targets (*HSPD1*, *HSPE1*, *HSPH1*, *CKS2*), *FBXW7* and *HSF1*, derived from microarray analysis of normal skin (n=4), primary (n=42) and metastatic melanoma (n=40) samples[58]. Whiskers represent the upper and the lower limits of the range. Boxes represent the first and third

quartile, and the line represents the median (unpaired *t*-test). (**c**) IHC staining with anti-FBXW7 and anti-HSF1 antibodies of the indicated tissue types (dysplastic nevi n=59, primary n=53 and metastatic n=53; $P<0.001$ for nevi FBXW7 versus HSF1, $P<0.01$ for primary FBXW7 versus HSF1, $P<0.05$ for metastatic FBXW7 versus HSF1; unpaired *t*-test; scale bar, 200 μm). (**d**) Kaplan-Meier survival curves of patients with tumors expressing high (2D, n = 76) or low levels of nuclear HSF1 (including 0, 1F and 1D, n = 101; $P= 0.01$; Log rank test). Staining was scored according to the intensity (0-2) and distribution (Focal <50%, Diffuse ≥50%). (**e**) *FBXW7* expression inversely correlates with HSF1 mRNA signature. *FBXW7*α (NM_033632) expression levels were measured by RNA-Seq in 325 Skin Cutaneous Melanoma (SKCM) samples from TCGA. HSF1 mRNA signature was defined as 1,864 mRNA expressions that were significantly correlated with HSF1 expression (NM_005526) with Spearman Correlation Coefficient > 0.3 and FDR < 5% in TCGA samples. Among them, 830 mRNAs with positive correlations were defined as the positive signature, while 1,034 mRNAs with negative correlations were defined as the negative signature. The first Principal Component (PC1) of the HSF1 positive signature was negatively correlated with *FBXW7*α expression (Spearman Correlation Coefficient = -0.4; $P< 0.001$); while the PC1 of the HSF1 negative signature was positively correlated with *FBXW7*α expression (Spearman Correlation Coefficient = 0.42; $P< 0.001$).

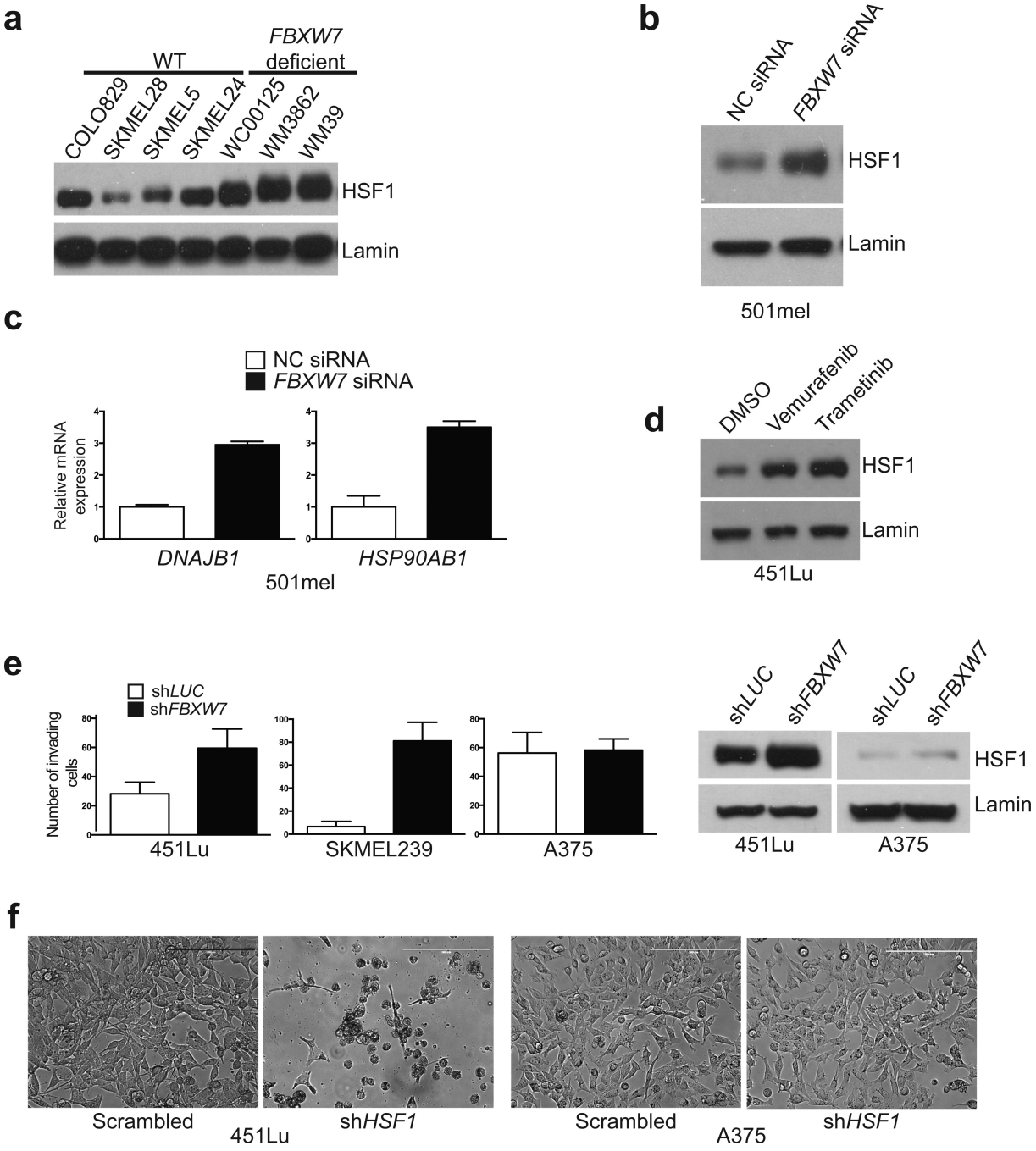

Figure 5. FBXW7 regulates nuclear HSF1 levels and invasion ability in human melanoma

(**a**) *FBXW7* deficiency stabilizes nuclear HSF1 in melanoma. Nuclear fractions from wild type (COLO829, SKMEL28, SKMEL5, SKMEL24) and deficient for *FBXW7* (WC00125, WM3862, WM39) melanoma cell lines were analyzed by immunoblotting as indicated. (**b**) *FBXW7* knockdown results in nuclear HSF1 accumulation. 501mel cells were treated with non-coding (NC) siRNA or siRNA against *FBXW7*. Nuclear fractions were analyzed by immunoblotting as indicated. (**c**) *FBXW7* knockdown results in increased HSF1 targets expression in melanoma. *DNAJB1* and *HSP90AB1* mRNA expression in 501mel cells

treated with non-coding (NC) siRNA or siRNA against *FBXW7* (*P*<0.001 for NC siRNA versus *FBXW7* siRNA; unpaired *t*-test, and n=3 independent experiments) (**d**) 451Lu cells were treated with the BRAF inhibitor Vemurafenib (2 μM, 9 h) and MEK inhibitor Trametinib (50 nM, 9 h). Nuclear fractions were analyzed by immunoblotting as indicated. (**e**) *FBXW7* depletion results in increased invasion in melanoma. 451Lu, SKMEL239 and A375 cells were infected with the indicated shRNA-encoding lentiviruses. One week after transduction, trans-well invasion assay was performed (*P*<0.05 for 451Lu sh*LUC* versus sh*FBXW7*, *P*<0.001 for SKMEL239 scrambled versus sh*FBXW7*, *P*>0.05 for A375 sh*LUC* versus sh*FBXW7*; n= 10 fields per biological replicate; 4 biological replicates; unpaired *t*-test). Nuclear fractions were analyzed by immunoblotting as indicated. (**f**) Representative microphotographs of 451Lu and A375 cells after 8 days of infection with the indicated shRNA-encoding lentiviruses (scale bar, 200 μm). Error bars indicate mean ± SD.. Uncropped blots are shown in Supplementary Fig. 8.

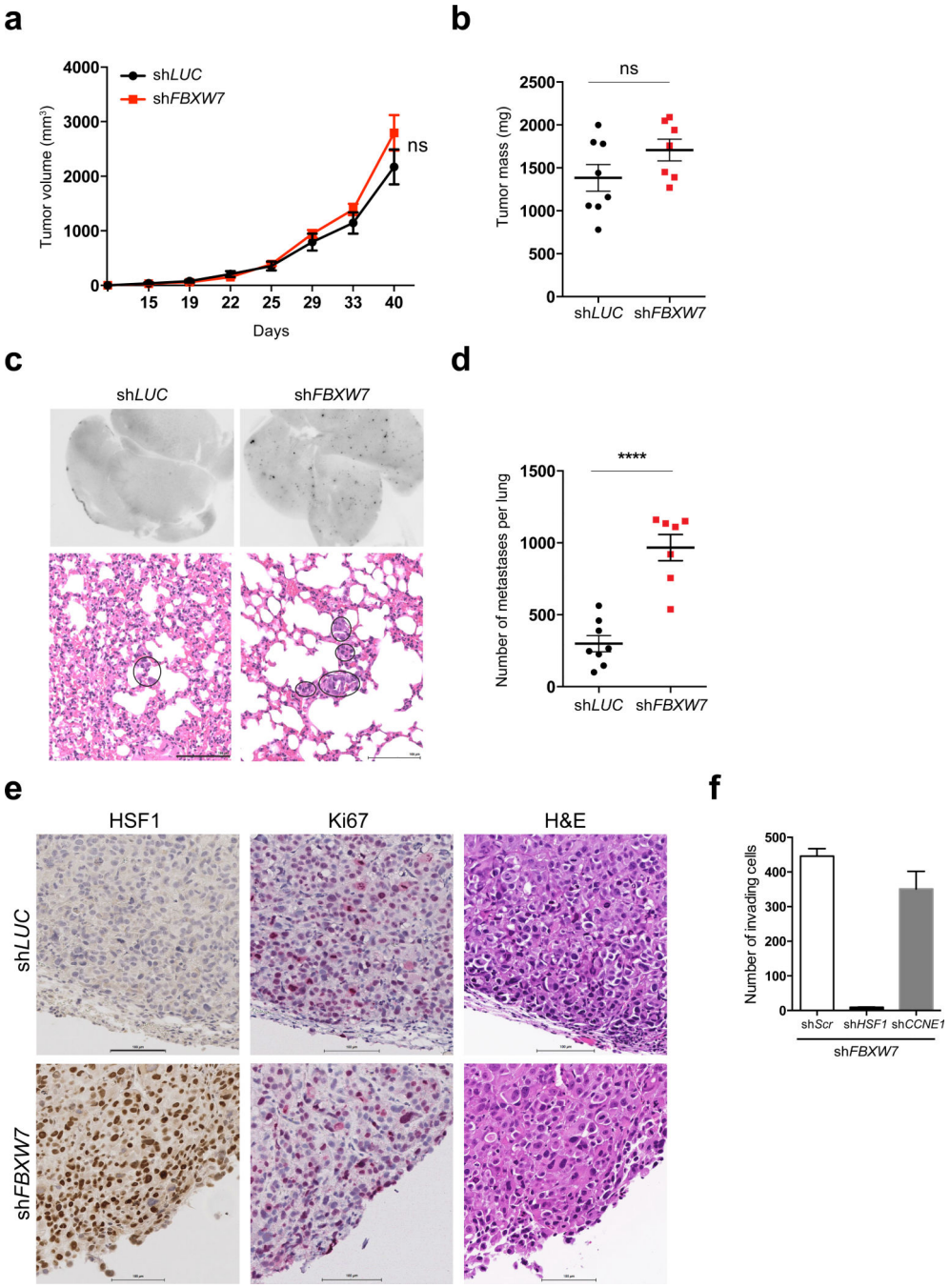

Figure 6. Nuclear HSF1 accumulation upon *FBXW7* depletion results in increased metastasis *in vivo*

In vivo metastasis assay with 451Lu cells transduced with control (sh*LUC*) or *FBXW7* shRNA injected subcutaneously in NOG/SCID mice. (**a**) *FBXW7* knockdown does not affect tumor growth or (**b**) tumor mass (sh*LUC*: n=8; sh*FBXW7*: n=7; n corresponds to number of mice per condition; ns: non significant; unpaired *t*-test) Error bars indicate mean ± SD. (**c**) Macroscopic pictures of mouse lungs and H&E-stained sections of lung metastases at termination of the experiment. Black circles mark metastatic foci (scale bar, 100 μm). (**d**)

Whisker plots show the number of metastases per lung. Mean ± SEM is depicted sh*LUC*: n=8; sh*FBXW7*: n=7; n corresponds to number of mice per condition).(****P<0.0001; unpaired *t*-test). (**e**) HSF1, Ki67 and H&E-stained sections of subcutaneous tumors resected at termination of the experiment show that *FBXW7* knockdown induces HSF1 nuclear accumulation but not proliferation (scale bar, 100 μm). (**f**) HSF1 is necessary for the increased metastatic potential of melanoma cells upon *FBXW7* depletion. 451Lu cells were transduced with control (sh*LUC*) or *FBXW7* shRNA. Melanoma cells that acquired increased metastatic potential were subsequently transduced with the indicated shRNA lentiviruses. Transwell invasion assay was performed 3 days after transduction (P<0.001 for sh*Scr* versus sh*HSF1*; n= 10 fields per biological replicate; 4 biological replicates; unpaired *t*-test). Error bars indicate mean ± SD.

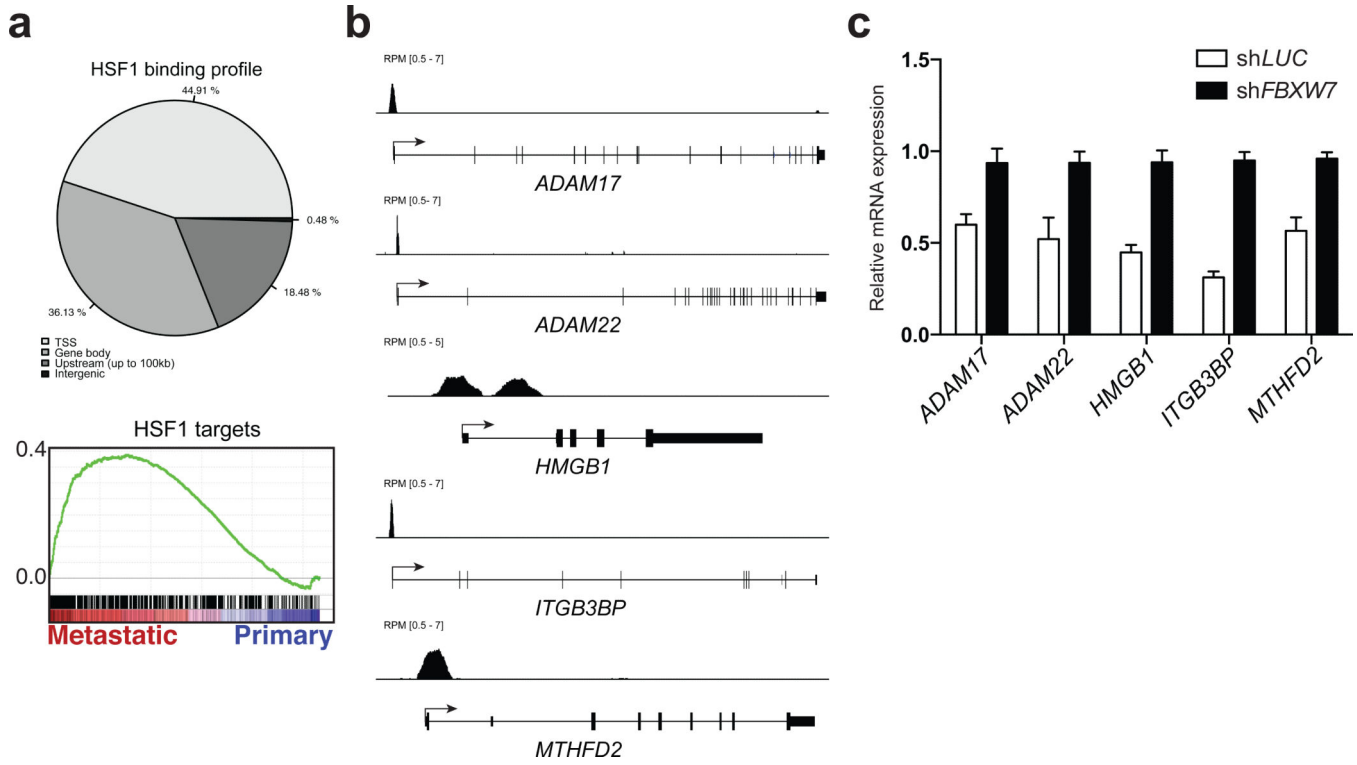

Figure 7. HSF1 drives a metastatic-supportive transcriptional program that is affected by *FBXW7* expression levels

(**a**) Genomic distribution of the regions of HSF1 occupancy (promoter, intragenic or intergenic). GSEA enrichment plot showing significant enrichment of the top 600 HSF1 targets for genes linked to metastasis in melanoma (Normalized Enrichment Score, NES=1.72; *P*=0.006). (**b**) Representative ChIP-Seq tracks of HSF1 metastasis-related targets. The scale corresponds to Reads Per Million (RPM). (**c**) mRNA expression analysis of HSF1 metastasis-related targets upon depletion of *FBXW7* (*P*<0.01 for sh*LUC* versus sh*FBXW7* for *ADAM17* or *ADAM22* or *MTHFD2* and *P*<0.001 for sh*LUC* versus sh*FBXW7* for *HMGB1* or *ITGB3BP*; unpaired *t*-test). Error bars indicate mean ± SD, and n=3 independent experiments.